# Optimal Origami Array Unfolding and Energy-Minimal Attitude Control for CubeSat Solar Wings

Justin Chang and Federico Baldan

## Abstract

*In this work, we propose novel control strategies for optimal constrained attitude control of a 3U Cubesat actuated by an origami-inspired solar panel structure serving as control surfaces to create differential drag. The optimal constrained attitude problem with differential drag is posed as convex subproblems through the Successive Convexification (SCVX) and Linear Matrix Inequality (LMI) reformulation for the non-convex keep-out zone constraints. To optimally reconfigure the solar panels folded in the Miura-ori patterns, Lagrangian mechanics is used to approximate the structure dynamics as a discrete function of control input and current states, which allows us to use SCVX to perform optimization to find the optimal reconfiguration strategies. Numerical experiments are performed to validate the proposed differential drag-based control, and the optimal origami reconfiguration also demonstrates the utilization of the system's potential energy to minimize the control efforts.*

## 1 Introduction

Solar-array deployment is one of the most critical phases of any space mission. A NASA Goddard analysis of flight data shows that incomplete or stalled deployments of solar arrays and other appendages are a principal cause of early satellite failure and capability loss[14].

In a more and more growing marked, the greater-Seattle area is considered to be the epicenter for space missions, allowing Washington State factories to assemble and project over half of all low-Earth-orbit satellites. Meanwhile, the trend over the next few years is clear: market analysts are predicting a demand for more than 11 000 new satellite launches between now and 2030. Companies are betting in new satellites and sustainable space technologies to envision a future where space will be more involved thanks to its logistic and efficiency advantages. For instance, Starcloud is developing orbital edge-compute nodes packed with GPU clusters whose kilowatt-plus power draw can only be met by roll-out, ultra-light blanket arrays that unfurl to several square metres from a 3-U envelope, whereas Starfish Space is building life-extension tugs whose hinged solar wings must repeatedly fold, latch, and redeploy to power successive rendezvous and docking cycles. In both scenarios large, lightweight panels must execute multiple fault-tolerant reconfigurations and maintain trajectory-efficient maneuvers a dual challenge that motivates the work presented here. Meanwhile, due to the easy access to the Very-LEO (VELO) with smaller launch vehicles and the reduced system requirements on the spacecraft, such as radioactive protection, sensor and communication requirements, the VLEO is becoming more attractive than ever to the Cubesat platform operators[10]. However, the VLEO environments pose unique challenges as the increased atmospheric disturbance makes the existing control strategies, including reaction wheels (RW), and magnetorquer (MTQ) suffer from motor saturation and a lack of enough control authority, respectively[10]. To address these challenges, many works on the active and passive aerodynamic attitude control have been proposed [3, 9, 2, 1, 5]. With the best knowledge of author; however, none of the previous work considered the optimality for drag reduction when performing the attitude maneuvering, which is a critical aspect for the VLEO spacecraft operation with the differential drag-based control system to increase the orbital lifespan. To make this control strategy more practical by taking the minimum drag control sequence, we developed novel optimal control methods by using the large solar panels fitted to the rear of the spacecraft to efficiently control the attitude of the small satellites in VLEO with an origami-inspired mechanism to fit these solar panels into a compact Cubesat and solve the offline optimal control problems through series of convex optimization subproblems. We also discovered a novel method to optimally reconfigure the origami structures to minimize the energy consumption.

This paper is organized as follows: In §2, we will present the clear definition of problems that will be solved; methods including SCVX an LMI reformulation used to solve the corresponding problems will be given in §3; we then present our findings in §4 before giving the final conclusion and suggestions for future works in §5.

## 2 Problem Statement

Aiming to this reliability problem, we visualize a Cubesat with a Miura-ori solar blanket tessellation. When folded, the blanket fits inside a 3-U volume; once deployed in orbit, it can be re-shaped based on demand to trade area for drag, torque, or thermal load. Fig. 2 illustrates the proposed 3U Cubasat with four foldable solar panels attached like badminton and the Miura-ori solar blanket tessellation. For the sake of the

clarity, we will consider two interconnected problems:

## 2.1 Description on the nature of this work

- **Optimal Miura-ori unfolding**: We want to find the minimum control effort unfolding process on the rigid Miura-ori Tessellation by controlling some selected creases. The closure loop, fixed length constraints, will be considered to prevent the origami from being torn apart. Simple actuator dynamics for rotating the folding angle will also be considered [7].

- **Optimal variable-geometry attitude control**: Once the solar panels composed of four Miura-ori Tessellations are fully deployed, they will act like control surfaces to create differential drag used for attitude control by rotating each individual panel. We are aiming to find the minimum rotation angles to achieve the targeted attitude while creating the minimum drag.

## 2.2 *Problem statement for the Miura-ori unfolding*

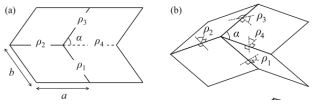

Figure 1: Single unit Miura-ori with folding angles $\rho_1, \rho_2$, sector angle $\alpha$, and edge lengths $a, b$ [6]

Refer to Fig. 1, let $\rho(t) = [\rho_1(t), \rho_2(t), \rho_3(t), \rho_4(t)]^T$ be the folding angles of Miura-ori base, and let each crease be a torsional spring with spring stiffness $k_i(t), i = 1, 2, 3, 4$. The small increment in the folding angles in the time interval $[t, t+1]$ is given by $\Delta\rho = \rho(t+1) - \rho(t)$. With the knowledge of the nominal angle of each spring defined by $\bar{\rho_i}$, we can calculate the total potential energy stored in each base by $U(t) = \sum_{i=1}^{4} \frac{1}{2} k_i(t)(\rho_i(t) - \bar{\rho_i(t)})$, and the gradient of energy is $d = \frac{\partial U}{\partial \rho}$. To simulate the origami dynamics, we need to define the Lagrangian to handle the geometry constraints (yes, just like constrained optimization!). We first need to define the closure loop constraints that relate the folding angle with sector angles $\varphi_i(t)$. The closure loop constraint is defined by:

$$F = T_{1,2} T_{2,3} T_{3,4} T_{4,1} = I^{3\times 3} \tag{1}$$

where

$$T_{i,i+1} = \begin{bmatrix} 1 & 0 & 0 \\ 0 & \cos\varphi_i & -\sin\varphi_i \\ 0 & \sin\varphi_i & \cos\varphi_i \end{bmatrix} \begin{bmatrix} \cos\rho_i & \sin\rho_i & 0 \\ -\sin\rho_i & \cos\rho_i & 0 \\ 0 & 0 & 1 \end{bmatrix} \tag{2}$$

We also need to define a few more variables to pave the way to construct the Lagrangian. Define the Jacobian $\frac{\partial F}{\partial \rho_i}|_\rho = J_i$, we denote $a_i = J_i[3,2], b_i = J_i[1,3], c_i = J_i[2,1]$, and the matrix

$$C = \begin{bmatrix} a_1 & a_2 & a_3 & a_4 \\ b_1 & b_2 & b_3 & b_4 \\ c_1 & c_2 & c_3 & c_4 \end{bmatrix} \tag{3}$$

Lastly, we have $\mathbf{r} = [F[3,2], F[1,3], F[2,1]]^T, H = diag([k_1(t), k_2(t), k_3(t), k_4(t)])$. The Lagrangian is then, finally, constructed in the quadratic form:

$$L(\Delta\rho, \lambda) = \frac{1}{2}\Delta\rho^T H \Delta\rho + d^T \Delta\rho + \lambda^T (C\Delta\rho + \mathbf{r}) \tag{4}$$

The term $\lambda^T(C\Delta\rho + \mathbf{r})$ is introduced to enforce the loop closure constraints, as described in [6]. Since the resulting formulation is the sequential quadratic programming with equality constraints and potential energy as the objective function, one can solve the optimal increment minimizing the potential energy by using Newton's SQP system with a closed-form solution [13]. Solving Newton's update law:

$$\begin{bmatrix} H & C^T \\ C & 0 \end{bmatrix} \begin{bmatrix} \Delta\rho \\ \lambda \end{bmatrix} = - \begin{bmatrix} d \\ r \end{bmatrix} \tag{5}$$

we have $\Delta\rho = -(H^{-1} - GCH^{-1}) - G\mathbf{r}$, $G = H^{-1}C^T(CH^{-1}C^T)^{-1}$. The origami dynamics can then be expressed by:

$$\rho(t+1) = \rho(t) - (H^{-1} - GCH^{-1}) - G\mathbf{r} \tag{6}$$

With the origami dynamics, we want to find the minimum control energy required to unfold the Miura-ori-based tessellation by controlling selected creases. Since the potential energy of each crease is $k_i(\bar{\rho_i} - \rho)$, we can achieve the minimum energy control by assuming we can change the nominal angle and spring stiffness of the controlled creases, which allows us to formulate the optimization problem:

$$\begin{aligned} \min_{\bar{\rho_c(t)}, k_c(t)} & \sum_{t=0}^{T-1} k_c(t)(\bar{\rho_c(t)} - \rho_c(t)) + \lambda|\rho_c(T) - \rho_{des}| \\ & \text{s.t.} \rho(t+1) = \rho(t) - (H^{-1} - GCH^{-1}) - G\mathbf{r}, \\ & |\text{dynamics constrains} \\ & |\bar{\rho_c(t)}| \le \pi |\text{spring direction constraint} \\ & 0 \le k_c(t) \le k_{max} |\text{spring stiffness constraint} \end{aligned} \tag{7}$$

where $\bar{\rho_c(t)}, k_c(t)$ are the controlled creases set. Since both the objective function and dynamics are not convex, we will linearize the objective function and used SCVX in [12] to solve the optimization problem.

### 2.3 *Problem statement for optimal attitude control with differential drag*

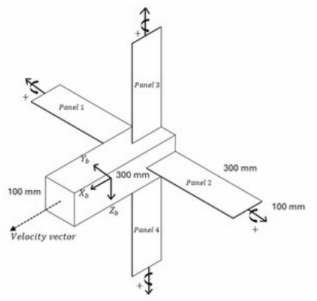


Figure 2: Illustration of a 3U Cubesat with four solar panels serving as actuators for attitude control [3]

Refer to the Fig. 2, let the states representing satellite dynamics be $x(t) = [\omega(t), q(t)]^T \in R^7$, and we define the unit quaternion $q(t) = [q_0(t), q_1(t), q_2(t), q_3(t)]^T$ and angular rates along body axes $\omega(t) = [\omega_1(t), \omega_2(t), \omega_3(t)]^T$. The control inputs $u(t) = [\phi_1(t), \phi_2(t), \phi_3(t), \phi_4(t)]^T$ are the rotational angles of each solar panel. The rigid body rotational dynamics in unitary quaternions with torque $\tau(t) \in R^3$ takes the form:

$$\begin{bmatrix}\dot{\omega}(t)\\ \dot{q}(t)\end{bmatrix} = \begin{bmatrix}J^{-1}(\tau(t) - \omega(t) \times (J\omega(t)))\\ \frac{1}{2}\Omega(t)q(t)\end{bmatrix} \tag{8a}$$

$$\Omega(t) = \begin{bmatrix} q_0(t) & -q_1(t) & -q_2(t) & -q_3(t) \\ q_1(t) & q_0(t) & q_3(t) & --q_2(t) \\ q_2(t) & -q_3(t) & q_0(t) & -q_1(t) \\ q_3(t) & q_2(t) & -q_1(t) & q_30(t) \end{bmatrix} \tag{8b}$$

where $J \in R^{3\times3}$ is the inertia matrix of the spacecraft. We discretize the spacecraft surfaces into fourteen flat surfaces and denote the unit vector perpendicular to the surface by $n_i \in R^3, i = 1\ldots, 14$, the arm (vector from the C.G. of the spacecraft to the geometry centroid) by $\ell_i \in R^3$. The total moment applied to the spacecraft is the sum of the individual moments on each surface and is given by:

$$\tau(t) = \sum_{i=1}^{14} \ell_i \times L_i \tag{9}$$

where $L_i = -A_i H(\cos\alpha_i)v^2\rho_{air}n_i \in R^3; A_i, v, \rho_{air} \in R^{++}, \alpha_i \in [-\pi, \pi]$ are force applied on each surface due to the aerodynamic force, surface area of each surface, relative velocity from space craft to the surrounding air (orbital velocity), and the local air density. We denote the desired attitude by $q_{des}$, and we want to minimize the attitude error $q_e = \|q(T) - q_{des}\|_2$ and the aerodynamic drag associated with the control surfaces $D(t) \propto \sum_{j=1}^4 \phi_j(t)$. We can formulate the optimal control problem as:

$$\begin{aligned}\min_{\phi(t)} &\sum_{t=0}^{T-1} ||\phi(t)||_2 + \beta\|q_{des} - q(T)\|_2 \\ &\text{s.t.} x(t+1) = g(x(t), \phi(t)) \text{|dynamics constraint} \\ &h(x(t)) \le 0 \text{|keepout zone constraint} \\ &|\phi_i(t)| \le \phi_{max}, \forall i \text{|rotation limits} \\ &\|\phi(t+1) - \phi(t-1)\| \le \dot{\phi}_{max}, \text{|rotational rate constraint}\end{aligned} \tag{10}$$

where $h(x) = \mathbb{R}e_1 z - \cos\theta_{half}$ is the attitude constraint function with $\mathbb{R} \in R^{3\times3}$ being the rotation matrix from body frame to LVLH frame, $z \in R^3$ denoting the unit vector representing the direction of keepout zone, and $\theta_{half}$ marking the half angle of the keepout zone. For how to actually solve the nonlinear and non-convex optimization problem, please refer to [12, 8] for how we transform the keepout zone constraints into LMI convex constraints and use SCVX to handle the nonlinear dynamics.

## 3 Methodologies

### 3.1 Linear Matrix Inequality (LMI) keep-out zone constraint reformulation

Recall the keep-out zone attitude constraint from Eq.10, which has the form of $v(t)^T w - \cos\theta \le 0$, where $v(t) \in R^3$ is the sensor vector in the inertia frame, $w \in R^3$ denotes the interference vector in the inertia frame, and lastly, $\theta \in [0, \pi]$ is the halfangle of the keep-out zone. The following shows an example of a keep-out zone.

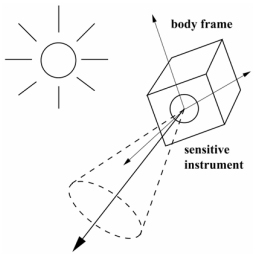


Figure 3: Illustration of keep out zone constraint [8]

Since the sensor vector is usually expressed in the body frame, we denote the sensor vector in the Brady frame as $v_B \in R^3$. The constraint can be reformulated as $q^T \bar{A} q \le 0$, where

$$\bar{A} = \begin{bmatrix} A & b \\ b^T & d \end{bmatrix} \tag{11a}$$

$$A = v_B w^T + w v_B^t - (v_B^T w + \cos\theta) I^{3\times3} \tag{11b}$$

$$b = w \times v_B \tag{11c}$$

$$d = v_B^T w - \cos\theta \tag{11d}$$

However, matrix $\bar{A}$ is indefinite, which makes the constraints nonconvex. In [8], the author proposed that the nonconvex

constraint can be posed equivalently as $q^T(A+\mu I)q \leq \mu$, and $\mu \in R$ is the scalar to ensure $(A+\mu I)$ is positive definite. The resulting constraint is then reformulated as a quadratic form, and by using the Schur complement, one can obtain

$$\begin{bmatrix} \mu & q^T \\ q & \mu I + \bar{A} \end{bmatrix} \succ 0 \tag{12}$$

as the keep-out zone constraint.

### 3.2 Nonlinear dynamics handling with Successive Convexification (SCVX)

SCVX is a trust region-based optimization method for dealing with non-convexity and nonlinearity. The principle of SCVX is to linearize the dynamics and constraints around the previous (or nominal) trajectory $(\mathbf{x}^i_{k-1}, \mathbf{u}^i_{k-1})$, and add the small perturbation $(\mathbf{d}^i_k, \mathbf{w}^i_k)$ regulated by the trust region $\mathbf{w}^i_k \leq \gamma^i_k$ to perturb the trajectory. In the SCVX, instead of solving the nonconvex and nonlinear objective and constraints, the "linear" penalty function will be considered:

$$\begin{aligned} &L(\mathbf{d}^i_k, \mathbf{w}^i_k, \mathbf{s}'^{ij}_k, \mathbf{v}^i_k) = C(\mathbf{x}^i_k + \mathbf{d}^i_k, \mathbf{u}^i_k + \mathbf{w}^i_k) + \\ &\sum_{t=0}^{T-1}[\lambda \|v^i_k(t)\|_1 + \sum_{j=1, j\neq i}^{N} \lambda \max(0, s^{ij}_k(t))] \end{aligned} \tag{13}$$

where

where $\mathbf{s}'^{ij}_k(t) = [s^{ij}_k(0), \ldots, s^{ij}_k(T)] \in \mathbb{R}^{T+1}$, $\forall i, j \in V, s'^{ij}_k(t) = s^{ij}_k(t) + \frac{\partial s^{ij}_k(t)}{\partial x^i(t)}|_{x^i_k(t)} d^i_k(t)$ are the slack variables for the nonconvex constraints violation, and the $\mathbf{d}^i_k \in \mathbb{R}^n, \mathbf{w}^i_k \in \mathbb{R}^m$ are the optimal increments of states and control over each optimization iteration, $\mathbf{v}^i_k = [v^i_k(0) \ldots, v^i_k(T)] \in \mathbb{R}^{n\times(T+1)}$, $v^i_k(t) = x^i_k(t+1) + d^i_k(t+1) - f(x^i_k(t), u^i_k(t)) - A^i_k(t)d^i_k(t) - B^i_k(t)w^i_k(t) \in \mathbb{R}^n$ are virtual control terms for accounting dynamic infeasibility resulting from the linearization of nonlinear dynamics, where $A^i_k(t), B^i_k(t)$ are the discrete matrix representations of the nonlinear, continuous system. The resulting linearized optimization problem from the SCVX is then given in the form of resembling the unconstrained problem, with the only constraint being the trust region.

$$\begin{aligned} \min_{(\mathbf{d}^i_k, \mathbf{w}^i_k, \mathbf{s}'^{ij}_k, \mathbf{v}^i_k)} \quad & L(\mathbf{d}^i_k, \mathbf{w}^i_k, \mathbf{s}'^{ij}_k, \mathbf{v}^i_k) \\ \text{s.t. } & \|\mathbf{w}^i_k\| \leq \gamma^i_k \end{aligned} \tag{14}$$

In our work, we don't use the original trust region updating mechanisms presented in [4, 11, 12], instead, we adopt a simpler method:

$$\gamma^i_{k+1} = \begin{cases} \frac{\gamma^i_k}{\omega_{SCVX}} & \text{if } L(\mathbf{d}^i_k, \mathbf{w}^i_k, \mathbf{s}'^{ij}_k, \mathbf{v}^i_k) < \\ & L(\mathbf{d}^i_{k+1}, \mathbf{w}^i_{k+1}, \mathbf{s}'^{ij}_{k+1}, \mathbf{v}^i_{k+1}), \\ \gamma^i_k & \text{otherwise} \end{cases}$$

where $\omega_{SCVX} > 1$ is the trust region decreasing ratio. The simplified SCVX algorithm is then given in Algorithm(1)

**Algorithm 1** SCVX with simplified trust region updating method

**procedure** INITIALIZATION($\mathbf{x}^i_0, \mathbf{u}^i_0$)
  Generate initial states (can be infeasible) $\mathbf{x}^i_0, \mathbf{u}^i_0$
**end procedure**
**procedure** MAIN LOOP($\mathbf{d}^i_k, \mathbf{w}^i_k, \mathbf{s}'^{ij}_k, \mathbf{v}^i_k$)
  **while** $\|\mathbf{x}^i_{k+1} - \mathbf{x}^i_k\| \geq Tol$ **do**
    Solve Eq.(14) to get $\mathbf{d}^i_k, \mathbf{w}^i_k$
    **if** $L(\mathbf{d}^i_k, \mathbf{w}^i_k, \mathbf{s}'^{ij}_k, \mathbf{v}^i_k)$
$\geq L(\mathbf{d}^i_{k+1}, \mathbf{w}^i_{k+1}, \mathbf{s}'^{ij}_{k+1}, \mathbf{v}^i_{k+1})$ **then**
      $\mathbf{x}^i_{k+1} \leftarrow \mathbf{x}^i_k + \mathbf{d}^i_k$
      $\mathbf{u}^i_{k+1} \leftarrow \mathbf{u}^i_k + \mathbf{w}^i_k$
      $\gamma^i_{k+1} \leftarrow \gamma^i_k$
    **else**
      $\mathbf{x}^i_{k+1} \leftarrow \mathbf{x}^i_k$
      $\mathbf{u}^i_{k+1} \leftarrow \mathbf{u}^i_k$
      $\gamma^i_{k+1} \leftarrow \frac{\gamma^i_k}{\omega_{SCVX}}$
    **end if**
  **end while**
  $\mathbf{x}^* \leftarrow \mathbf{x}^i_{k+1}, \mathbf{u}^* \leftarrow \mathbf{u}^i_{k+1}$
  **Return** $\mathbf{x}^*, \mathbf{u}^*$
**end procedure**

Throughout this work, we will use SCVX to handle all the nonlinearity dynamic constraints.

## 4 Results

In this section, we will present the main results for both optimal attitude control with differential drag and the optimal reconfiguration of the origami structure.

### 4.1 Optimal solar panel unfolding

We present the optimal solar panel unfolding process in this section. Table. 1 shows the universal parameters used across numerical simulations for optimal origami unfolding. All the case-specific parameters used in the Miura-ori unfolding process are given in the Table.2. For the last case of optimal unfolding with three Miura-ori bases, all the parameters are the same as in case 2, and the controlled creases are highlighted in the Fig.5

Table 1: Universal optimization setting parameters

| | **Values** |
|---|---|
| **SCVX trust regions** $(r_{\bar{\rho}}, r_k)$ | $1\ deg, 100\ N/m$ |
| **Trust region reduction ratio** $\omega_{scvx}$ | 1.05 |
| **Total simulation steps** | 301 |

Table 2: Simulation parameters for each case

| **Case 1: single base unfolding** | **Values** |
|---|---|
| **Initial spring stiffness** $k_i, i = 1, 2, 3, 4$ | $1000\ N/m$ |
| **Sector angle** $\alpha$ | $\pi/4\ rad$ |
| **Initial folding angles** $[\rho_1, \rho_2, \rho_3, \rho_4]$ | $[179, 179, 179, -179]\ deg$ |
| **Case 2: Optimal unfolding control with single base** | **Values** |
| **Initial spring stiffness** $[k_1(0), k_2, k_3, k_4]$ | $[2, 2, 2, 2] * 10^3\ N/m$ |
| **Target folding angle** $\rho_{1,des}$ | $5\ deg$ |
| **Terminal cost constant** $\lambda$ | 100000 |

From Fig. 4, the result illustrates that the minimum energy configuration corresponds to the unfolded configuration.

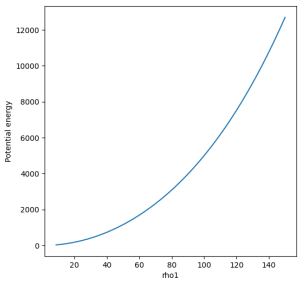


Figure 4: Unfolding process of the solar panels with Miura-ori patterns. Fully folded (top), unfolded (middle), and side view (bottom)

In the second case, where two springs are controlled, one can see that the controlled springs are partially driven by other springs in the beginning, and later will actively introduce more energy into the system to drive the origami to the desired configuration in a given time, which can be seen from the distinct potential energy difference between springs.

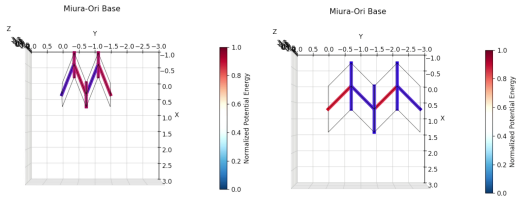


Figure 5: Unfolding process of the solar panels with Miura-ori patterns. Fully folded (top), unfolded (middle), and side view (bottom)

Figure 6 shows different physical quantities of the single base case, and one can notice the initial increase in the potential energy is required to ensure target terminal states can be reached. The rapid decline in the potential energy of the controlled spring also clearly shows the minimization of control energy.

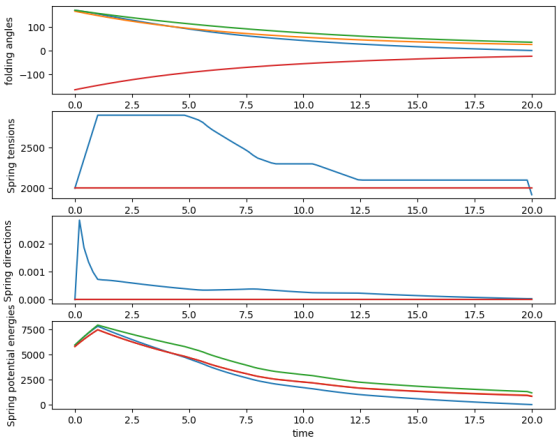


Figure 6: Unfolding process of the solar panels with Miura-ori patterns. Fully folded (top), unfolded (middle), and side view (bottom)

Lastly, we implemented this unfolding animation on the 3U platform, demonstrating how this mechanism can be integrated into a Cubesat.

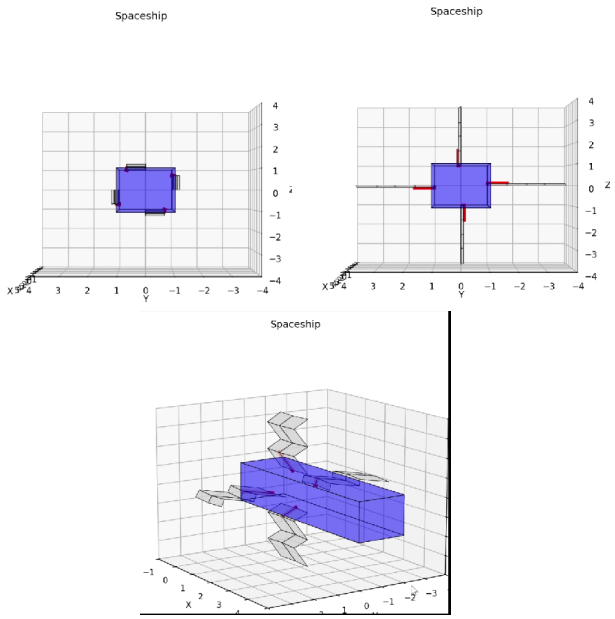


Figure 7: Unfolding process of the solar panels with Miura-ori patterns. Fully folded (top), unfolded (middle), and side view (bottom)

## 4.2 Optimal keepout zone constrained attitude control with differential drag

In the end, we also implemented the optimal control algorithm for the differential drag-controlled Cubesat. Fig.8 shows the attitude maneuvering of the differential drag controlled 3U Cubesat with the keep-out zone constraints. Fig. 9 presents the time history of the solar panel rotational angles.

Table 3: Simulation parameters for optimal attitude control problem

| | **Values** |
|---|---|
| **Atmospheric density** | $2.468e-11\ kg/m^3$ |
| **Orbital rate** ($200\ km$) | $7\ km/s$ |
| **Inertia** ($I_{xx}, I_{yy}, I_{zz}$) | $0.01, 0.02, 0.02$ $kg \cdot m^2$ |
| **Keep out zone attitude(raw, pitch,yaw)** | $[0, 15, 5]\ deg$ |
| **Keep out zone half angle** | $15\ deg$ |
| $\phi_{max}$ | $25\ deg$ |
| **SCVX trust region** | $0.1$ |
| **Trust region reduction ratio** $\omega_{scvx}$ | $1.1$ |
| **Final time** $T$ | $120\ s$ |
| **Time increment** $dt$ | $0.2\ s$ |

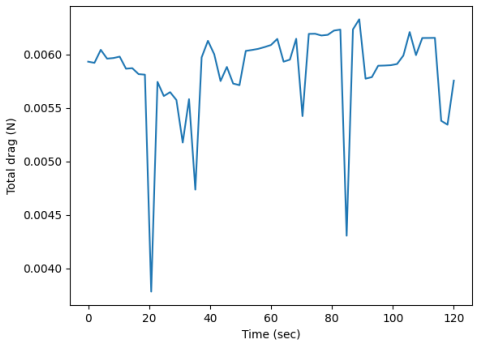


Figure 10: Total atmospheric drag experienced over time

The total drag experienced during the course of maneuvering is shown in Fig.10. Table. 3 summarizes the parameters used in the attitude trajectory numerical simulation.

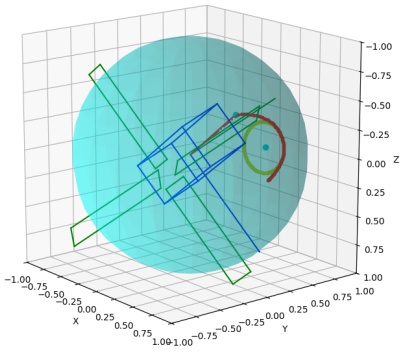

Figure 8: Optimal constrained attitude control with differential drag. The yellow circle is the keepout zone

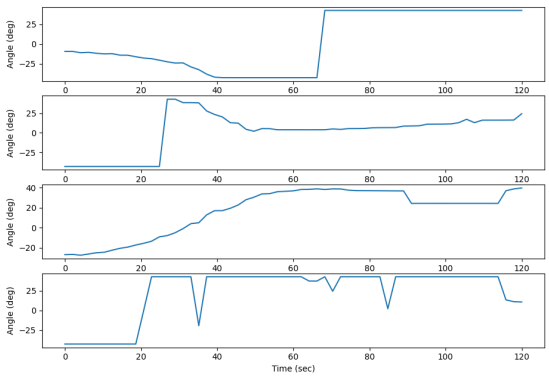


Figure 9: Solar panel rotation angles during the attitude maneuvering

# 5 Conclusion

In this work, we discovered the possibility of using solar panels to serve as the control surfaces on the airplane to adjust the attitude in VLEO environments; we also demonstrated by using the Miura-pri origami patterns, we can fit the large size solar panels in a compact 3U platform with the minimum energy controller to unfold them. The LMI reformulation and SCVX enable the efficient attitude trajectory planning, while the Lagrangian mechanics allow us to formulate the optimal reconfiguration problem into a series of convex subproblems. Our research will enable the VELO Cubesat operation to be more feasible with reduced system complexity of ADCS with the improved control authority compared to other existing control strategies in VELO.

In future work, we will also explore the controllability of the origami structures to place the actuators on the right creases to design the optimal self-actuated origami structure and how the states can be assessed through the observability analysis.

# References


[1] J. Auret and Willem Steyn. Design of an aerodynamic attitude control system for a cubesat. *62nd International Astronautical Congress 2011, IAC 2011*, pages 9009–9017, 2011. 1

[2] Valentín Cañas, D González, Jonathan Becedas, Rosa Dominguez, Peter Roberts, Nicholas Crisp, Vitor Oiko, S Edmondson, Stephen Worrall, Sarah Haigh, Katharine Smith, Rachel Lyons, Sabrina Livadiotti, C Huyton, Luciana Sinpetru, Silvia Donaire, Daniel García-Almiñana, M Nieto, C Muñoz, and B. Heisserer. Attitude control for satellites flying in vleo using aerodynamic surfaces. *Journal of the British Interplanetary Society*, pages 103–112, 2020. 1

[3] Cheng Chang, Robert Breidenthal, Bo-Chuan Lin, and Ya-Xun Yang. [ssc24-wi-03] aerodynamic satellite attitude control in very low earth orbit. 08 2024. 1, 3

[4] Purnanand Elango, Dayou Luo, Abhinav G. Kamath, Samet Uzun, Taewan Kim, and Behçet Açıkmeşe. Successive convexification for trajectory optimization with continuous-time constraint satisfaction, 2024. 4

[5] Michael Gargasz. Optimal spacecraft attitude control using aerodynamic torques. page 91, 2007. 1

[6] Yucai Hu and Haiyi Liang. Folding simulation of rigid origami with lagrange multiplier method. *International Journal of Solids and Structures*, 202:552–561, 2020. 2

[7] Gangshan Jing, Changhuang Wan, Ran Dai, and Mehran Mesbahi. Design and transformation control of triangulated origami tessellation: A network perspective. *IEEE Transactions on Network Science and Engineering*, 11:635 – 647, 01 2024. 2

[8] Yoonsoo Kim, Mehran Mesbahi, Gurkirpal Singh, and Fred Y. Hadaegh. On the convex parameterization of constrained spacecraft reorientation. *IEEE Transactions on Aerospace and Electronic Systems*, 46(3):1097–1109, 2010. 3

[9] Sabrina Livadiotti, Nicholas H. Crisp, Peter C. E. Roberts, Vitor T. A. Oiko, Simon Christensen, Rosa Maria Domínguez, and Georg H. Herdrich. Uncertainties and design of active aerodynamic attitude control in very low earth orbit. *Journal of Guidance, Control, and Dynamics*, 45:859–874, 2022. 1

[10] J. Virgili Llop, P.C.E. Roberts, Zhou Hao, L. Ramio Tomas, and V. Beauplet. Very low earth orbit mission concepts for earth observation: Benefits and challenges. 2014. Reinventing Space Conference ; Conference date: 18-11-2014 Through 20-11-2014. 1

[11] Yuanqi Mao, Daniel Dueri, Michael Szmuk, and Behçet Açıkmeşe. Successive convexification of non-convex optimal control problems with state constraints. *IFAC-PapersOnLine*, 50(1):4063–4069, 2017. 20th IFAC World Congress. 4

[12] Yuanqi Mao, Michael Szmuk, Xiangru Xu, and Behcet Acikmese. Successive convexification: A superlinearly convergent algorithm for non-convex optimal control problems, 2019. 2, 3, 4

[13] Michael J. O'Neill. A two stepsize sqp method for nonlinear equality constrained stochastic optimization, 2024. 2

[14] Alejandro Rivera and Alphonso Stewart. Study of spacecraft deployables failures. Technical report, KBR Inc. / NASA Goddard Space Flight Center, Greenbelt, MD, USA, 2020. KBR Inc. / NASA GSFC Bldg. 29 Rm 100 and Bldg. 7 Rm 158. 1